

Article

Specific Sensitivity Analysis and Imitative Full Stress Method for Optimal BCCZ Lattice Structure by Additive Manufacturing

Haonan Li ¹, Weidong Yang ^{1,*} , Qianchao Ma ¹, Zhihan Qian ¹ and Li Yang ^{2,*}¹ School of Mechanical Engineering, Hebei University of Technology, Tianjin 300401, China² Department of Industrial Engineering, University of Louisville, Louisville, KY 40292, USA

* Correspondence: yangweidong@hebut.edu.cn (W.Y.); li.yang.1@louisville.edu (L.Y.)

Abstract: Additive manufacturing (AM) can quickly and easily obtain lattice structures with light weight and excellent mechanical properties. Body-centered cubic (BCC) lattice structure is a basic type of lattice structure. BCC with Z strut (BCCZ) lattice structure is a derivative structure of BCC lattice structure, and it has good adaptability to AM. Generally, the thickness of each pillar in the BCCZ lattice structure is uniform, which results in the uneven stress distribution of each pillar. This makes the potential of light weight and high strength of the BCCZ lattice structure not fully played, and the utilization rate of materials can be further improved. This paper designs an optimization method. Through the structural analysis of a BCCZ lattice structure, an optimization method of a BCCZ lattice structure based on parametric modeling parameters is presented. The section radius of all pillars in the BCCZ lattice is taken as a design variable, and the specific sensitivity analysis method and simulated full stress optimization idea are successively used to determine the optimal section radius of each pillar. Finally, the corresponding model is designed and samples are manufactured by LPBF technology for simulation and experimental verification. The results of simulation and experiment show that the strength limit of the optimized parts increased by 18.77% and 18.43%, respectively, compared with that before optimization.

Keywords: additive manufacturing; lattice structures; BCCZ; specific sensitivity analysis; imitative full stress method



Citation: Li, H.; Yang, W.; Ma, Q.; Qian, Z.; Yang, L. Specific Sensitivity Analysis and Imitative Full Stress Method for Optimal BCCZ Lattice Structure by Additive Manufacturing. *Crystals* **2022**, *12*, 1844. <https://doi.org/10.3390/cryst12121844>

Academic Editors: Hao Yi, Huajun Cao, Menglin Liu and Le Jia

Received: 24 November 2022

Accepted: 14 December 2022

Published: 16 December 2022

Publisher's Note: MDPI stays neutral with regard to jurisdictional claims in published maps and institutional affiliations.



Copyright: © 2022 by the authors. Licensee MDPI, Basel, Switzerland. This article is an open access article distributed under the terms and conditions of the Creative Commons Attribution (CC BY) license (<https://creativecommons.org/licenses/by/4.0/>).

1. Introduction

Based on the principle of discrete stacking, AM realizes model design through computer aided design (CAD) and direct manufacturing driven by 3D data [1]. As an advanced manufacturing technology, AM has subverted the traditional manufacturing concept and has incomparable unique advantages in manufacturing complexity and special structures, bringing conceptual innovation to the entire manufacturing industry [2]. Compared with traditional manufacturing methods, AM makes up for the vacancy of traditional manufacturing methods, enabling parts that in the past were difficult to manufacture or could not be manufactured or had high manufacturing costs to be processed and manufactured [3]. One of the most outstanding advantages of AM is that it increases the degree of freedom of design, which is very helpful for the manufacturing of lattice structures. In the past two decades, AM has been rapidly developed and applied. Powder bed fusion (PBF) is a group of AM techniques. When equipped with lasers as energy sources, the processes are also known as laser powder bed fusion (LPBF). LPBF is also commercially known as selective laser melting (SLM) or direct metal laser melting, which is shown in Figure 1 [4]. LPBF can fabricate complex components by melting metal powders layer by layer using a high-energy laser beam and generally can be used for producing complicated parts [5]. The forming size is getting smaller and smaller, reaching the millimeter level. The printing material has also achieved the transition from the past titanium alloy to the present aluminum alloy [6]. At the same time, relevant enterprises around the world have also begun to increase

the research and development of AM equipment, and have made relatively successful progress, and are gradually realizing the commercialization of AM equipment [7]. With the upgrading and development of AM equipment, the gap between structural design and manufacturing has been further narrowed, and the manufacturing problems of millimeter scale complex structures have been solved. Structural design benefiting from AM has gradually entered the perspective of designers [8]. The design method for AM reduces the manufacturing constraints in the traditional design concept, making the forming of millimeter scale complex structures more simple and direct forming possible, which helps to achieve parametric control of complex structures [9]. The lattice structure benefits from the development of AM, and its shortcomings that were difficult to manufacture in the past have been solved to a large extent. It has many characteristics such as light weight, high strength, excellent energy absorption, good thermal performance, sound insulation and noise reduction, and biocompatibility [10–13]. Different from the traditional civil construction industry, the lattice structure oriented to AM is usually at the millimeter level. The appearance of AM makes the lattice structure design break through the size constraints and can realize the design and manufacturing at the millimeter level [14]. In recent years, successful cases of the combination of lattice structure design and AM have been emerging, and the feasibility of this scheme is constantly being verified. The emergence and development of AM provide a new solution to the problem that the lattice structure has been difficult to be manufactured by traditional manufacturing methods, and provide support and help for the design of millimeter level lattice structure [15–17].

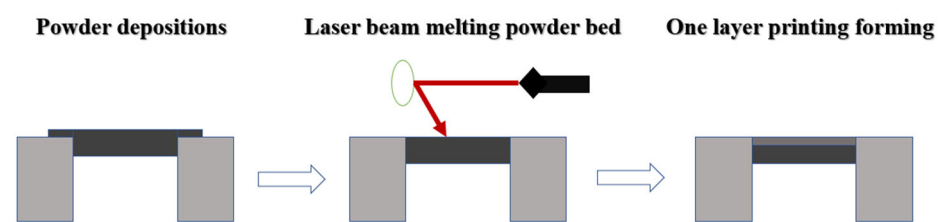


Figure 1. Laser powder bed fusion process.

The research on the combination scheme of AM and lattice structure design in aerospace [18], automotive industry [19], biomedicine [20] and other aspects shows that AM and lattice structure design show a very broad development prospect in the field of light weight. With the help of AM, the design model of lattice structure has been greatly guaranteed for manufacturing, and the lattice structure design for AM also provides researchers with greater imagination space. At the same time, the steps of the entire AM process are more concise, which can greatly save manufacturing time and reduce manufacturing costs from the design end of the computer equipment to the manufacturing equipment [21]. The lattice structure produced by AM can meet the size and shape requirements and achieve millimeter level precision manufacturing, greatly ensure the performance requirements, reduce material loss and improve material utilization. In economic development, large machines (such as aircraft, automobiles, etc.), after using the parts produced by the lattice structure design scheme for AM, reduce their own weight and energy consumption, so as to reduce all kinds of pollution caused by energy consumption and help to achieve green development with AM as the core [22].

BCC lattice structure is characterized by simple topology, strong designability, strong manufacturability, and excellent mechanical properties [23]. Moreover, it is worth noting that the success rate of BCC lattice structure in AM is very high in millimeter scale manufacturing, which is mainly due to the tilt angle of the pillar in the BCC lattice structure. Leary et al. [24,25] quantified manufacturability of aluminum lattice strut elements by experiment. They set four possible strut inclination angles: 0, 35.26, 45 and 90 degrees in a unit cell with equal side length and found that the manufacturability of struts at other angles was well beyond 0 degrees. BCCZ lattice structure is a derivative structure of BCC lattice structure. On the basis of retaining the advantages of BCC lattice structure with strong design, good

manufacturing and a high success rate in AM, its related performance has been greatly improved compared with BCC lattice structure due to the existence of a strengthened Z pillar [26–28]. Chua et al. [29] used the finite element analysis method to study the mechanical properties of lattice structure in order to avoid cracks and pores that may occur in the process of AM. Chen et al. [30] used the MIST optimization algorithm to optimize the pillar size inside the cell. Jin et al. [31] completed the parametric design by obtaining the cell length diameter ratio distribution matrix and mapping the matrix to the pillar size of the unit cell. In the above research, the manufacturability and optimization methods of struts in lattice structures were studied. However, in the current research, the optimization design of the BCCZ lattice structure for AM needs to be strengthened. At present, the thickness of each pillar in the BCZZ lattice structure is uniform, which easily leads to uneven stress distribution of each pillar. The advantage of the BCCZ lattice structure in light weight and great strength has not been fully utilized, and the utilization rate of materials can be further improved in order to further take advantage of the combination of AM and lattice structure to better release constraints. This paper takes BCCZ lattice structure as the research object. On the basis of a structural analysis of the BCCZ lattice structure, the section radius of all pillars in the BCCZ lattice structure is taken as the design variable. A BCCZ lattice structure optimization method based on the combination of specific sensitivity analysis and the idea of imitative full stress is proposed to maximize the material utilization of each pillar in the BCCZ lattice structure. Last, the optimization method in this paper is explained and verified by finite element simulation and experiment. Through the designed method in this paper, the dangerous stress in the BCCZ structure can be controlled within the allowable stress range, and the strength of the whole structure can be improved. The designed BCCZ structure can maintain better strength on the basis of light weight.

2. Analysis of BCCZ Lattice Structure

The lattice structure can be seen as a porous structure composed of many cells according to the set distribution rules. Chen et al. [32] summarized that the unit cell had an important impact on the characteristics of lattice structures, such as mechanical response, specific surface area, stiffness, pore size. Therefore, the unit cell is very representative in the lattice structure analysis [33]. Therefore, this section analyzes the BCCZ lattice structure from the perspective of the BCCZ unit cell.

2.1. BCCZ Unit Cell Topology Analysis

The BCCZ lattice structure is generally composed of BCCZ cells through X, Y and Z arrays. Figure 2 shows the BCCZ lattice structure and its corresponding unit cell structure diagram. The BCCZ lattice structure in Figure 2a is generated by BCCZ cells in Figure 2b through repeated arrays in X, Y and Z directions, and contains $5 \times 3 \times 2$ cells, respectively.

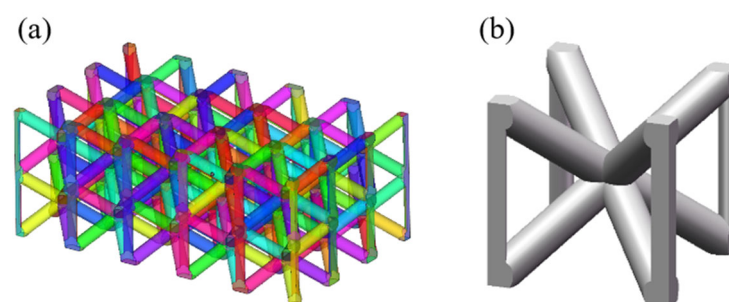


Figure 2. (a) BCCZ lattice structure diagram; (b) BCCZ unit cell diagram.

As shown in Figure 2a, the BCCZ lattice structure composed of BCCZ cells can be regarded as a micro truss structure, whose structural elements are composed of pillars and nodes. The topological structure of the BCCZ unit cell has little change compared with the BCC unit cell. Figure 3 shows the topology of the BCC unit cell and BCCZ unit cell, as well

as the numbering sequence of nodes and pillars inside the unit cells. The BCC unit cell central node (N9) and 8 outer nodes (N1–N8) are connected in the form of pillars, and the location of the central node is determined by Formula (1). On the basis of inheriting the topological configuration of the BCCZ unit cell, the BCCZ unit cell can be constructed by adding a strengthened Z pillar in the direction parallel to the load. That is, on the basis of node N1–N9, add P9 to P12 between nodes N1 to N5, N2 to N6, N3 to N7, and N4 to N8.

$$\begin{cases} x_9 = \frac{1}{8} \sum_{i=1}^8 x_i \\ y_9 = \frac{1}{8} \sum_{i=1}^8 y_i \\ z_9 = \frac{1}{8} \sum_{i=1}^8 z_i \end{cases} \quad (1)$$

where (x_9, y_9, z_9) is the coordinate of central node N9, and (x_i, y_i, z_i) corresponds to the coordinate of outer nodes N1–N8.

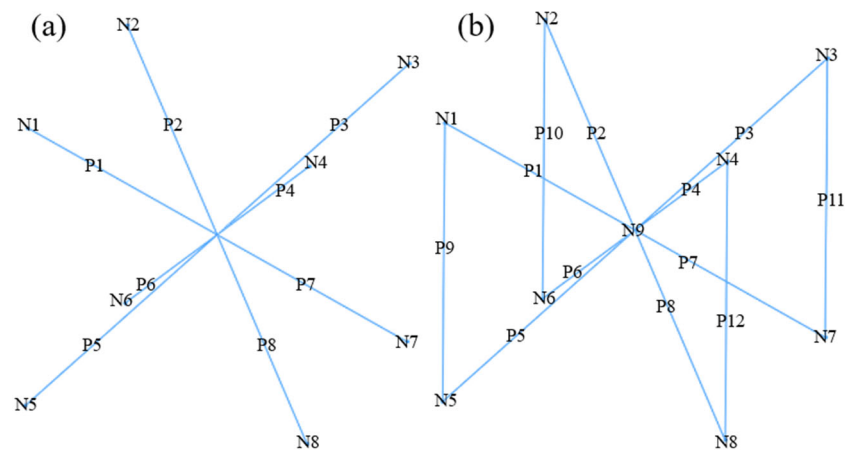


Figure 3. Topological structure comparison diagram of BCC unit cell and BCCZ unit cell and numbering sequence of each pillar: (a) BCC; (b) BCCZ.

2.2. Parametric Modeling

The topological analysis of Section 2.1 is helpful to realize the parametric modeling of the BCCZ unit cell, and then the parametric modeling of the BCCZ lattice structure can be realized. In the current research, the modeling precondition is to set the section shape of the BCCZ lattice structure pillar as a circle, and the external geometry of BCCZ unit cell as a cube [34].

Figure 4 shows the BCCZ lattice structure decomposition steps. The BCCZ lattice structure can be divided into many BCCZ cells. The BCCZ unit cell can be divided into eight inclined pillars of cylinders and four outer pillars of 1/4 cylinders. Among them, each outer pillar intersects two inclined pillars, and eight inclined pillars intersect at the central node. The side length of the cell is set as S , the length of the inclined pillar is $l_i (i = 1, 2, \dots, 8)$, the section radius of the inclined pillar is $r_i (i = 1, 2, \dots, 8)$, the length of the outer pillar is $l'_i (i = 9, 10, 11, 12)$, and the section radius of the outer pillar is $r'_i (i = 9, 10, 11, 12)$. Formulas (2)–(4) show the fixed geometric relationship in the BCCZ unit cell:

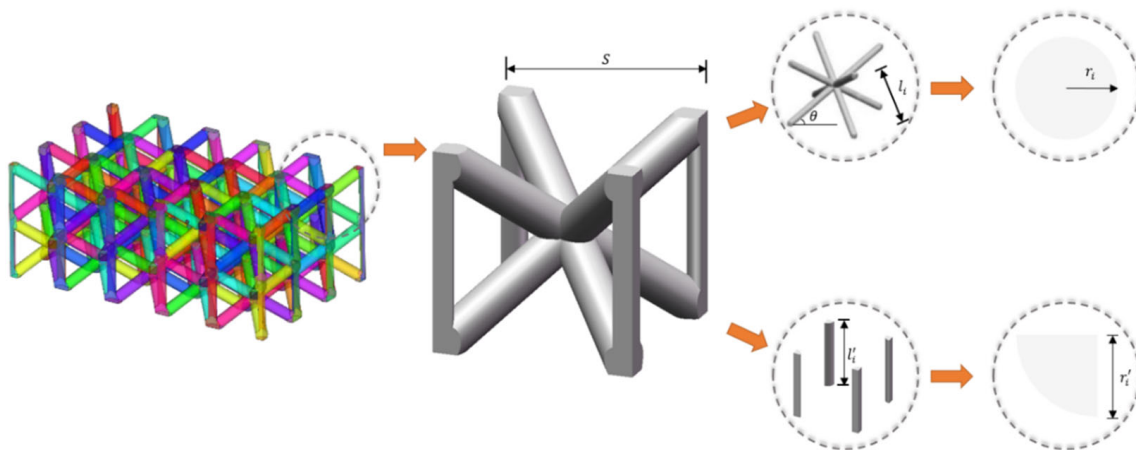


Figure 4. Analysis of design parameters of BCCZ lattice structure.

- (1) Inclined pillar length l_i and unit cell side length S :

$$l_i = \frac{\sqrt{3}}{2} S \quad (2)$$

- (2) Outer pillar length l'_i and unit cell side length S :

$$l'_i = S \quad (3)$$

- (3) Angle between inclined pillar and horizontal direction θ :

$$\theta = \sin^{-1} \frac{1}{\sqrt{3}} \quad (4)$$

To sum up, the parametric modeling of the BCCZ unit cell can be completed through unit cell side length S , the section radius r_i ($i = 1, 2, \dots, 8$) of the inclined pillar and the section radius r'_i ($i = 9, 10, 11, 12$) of the outer pillar. By assigning the above design parameters, BCCZ cells with different structural parameters can be obtained. The BCCZ unit cell is an outstanding representative of the BCCZ lattice structure. According to the structural relationship between the two, the structural parameters of the BCCZ lattice structure can be summarized as unit cell side length S , the section radius r_i ($i = 1, 2, \dots, 8$) of the inclined pillar, the section radius r'_i ($i = 9, 10, 11, 12$) of the outer pillar, X , Y and the number of cells in Z direction x , y and z .

3. Optimization Method

The current optimization of lattice structure can be summarized in the following two aspects. On the one hand, a few researchers changed the cell strut into a curve by removing the constraint that the section radius of the cell strut is equal everywhere. On the macro level, it reflects that the shape of the lattice structure pillar has changed, and the optimization at the cell level has been realized by reducing the impact of stress concentration, which has realized the innovation of cell configuration to a certain extent [35]. On the other hand, because it is difficult to propose new unit cell configurations, most researchers still use various optimization methods (such as topology optimization) to optimize and design lattice structures with better performance on the basis of existing unit cells [36,37]. According to the above two kinds of optimization ideas, this paper synthesizes their respective characteristics, and on the basis of the existing cell elements and the analysis in Section 2, takes the section radius of each pillar of BCCZ lattice structure as an independent design variable and relieves the constraint that the section radius between the pillars is equal. A BCCZ lattice structure optimization method combining specific sensitivity analysis and imitative full stress design method is proposed. Figure 5 shows the design process of this method.

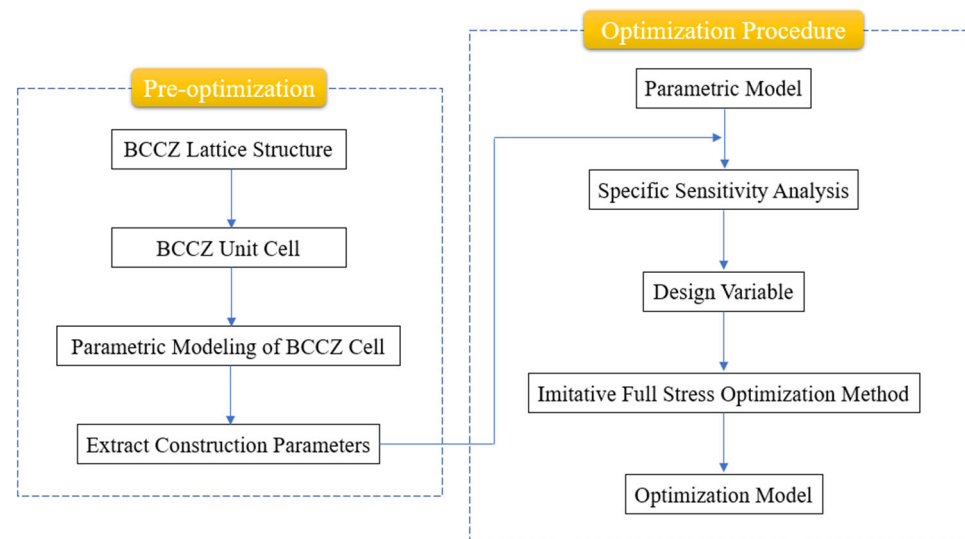


Figure 5. Procedures for the optimization design of specific sensitivity analysis and imitative full stress design.

3.1. Specific Sensitivity Analysis

According to the analysis in Section 2.2, the number of pillars of the BCCZ lattice structure is large, which leads to many variables to be designed. As a result, BCCZ lattice structure optimization is difficult to design, and complex design problems and a reasonable optimization design scheme are difficult to determine. To solve this problem, this paper uses the method of specific sensitivity analysis to distinguish the design variables and solve the optimization direction of each design variable, so as to carry out the follow-up optimization work.

The concept of sensitivity is often used in rigid frame structures in practical projects. It can be used to express the degree of influence on a certain performance of the overall structure when a variable changes [38]. In this paper, the design variable is the section radius of each pillar of the BCCZ lattice structure, that is, the section radius r_i of inclined pillar and the section radius r'_i of outer pillar, and the influence performance can be a mechanical property of the BCCZ lattice structure [39]. The mathematical model of sensitivity is shown in Formula (5).

$$P = p(r_1, \dots, r_i, \dots, r_m, r'_1, \dots, r'_i, \dots, r'_n) \quad (5)$$

where P is the performance function of BCCZ lattice structure, m is the number of inclined pillars and n is the number of outer pillars.

The change in the BCCZ lattice structure performance caused by the increment dr_i or dr'_i of any pillar section radius change is dP , namely:

$$dP = \frac{\partial p}{\partial r_1} dr_1 + \dots + \frac{\partial p}{\partial r_i} dr_i + \dots + \frac{\partial p}{\partial r_m} dr_m + \frac{\partial p}{\partial r'_1} dr'_1 + \dots + \frac{\partial p}{\partial r'_i} dr'_i + \dots + \frac{\partial p}{\partial r'_n} dr'_n = \sum_{i=1}^m \frac{\partial p}{\partial r_i} dr_i + \sum_{i=5}^n \frac{\partial p}{\partial r'_i} dr'_i \quad (6)$$

where the partial derivative of the performance function P of the BCCZ lattice structure to the section radius r_i or r'_i of the pillar is the performance sensitivity of the BCCZ lattice structure.

The performance sensitivity analysis can be used to determine the design variables that have a significant impact on the overall performance of the BCCZ lattice structure among the BCCZ lattice structure optimization design variables, and formulate an optimization design scheme to improve the optimization efficiency. However, the advantage of the BCCZ lattice structure over strength cannot be fully exploited by analyzing performance sensitivity only. Xu et al. [40] designed some lattice structures with different relative densities (0.15–0.5) and carried out experimental monitoring. They systematically studied

the effect of relative density on the compressive properties of lattice structures, including mechanical properties, failure mechanisms and energy absorption capacity. The results show that the compressibility of the lattice structure changes significantly with the change of the relative density, and the performance of the lattice structure can usually be improved by simply increasing the section radius. In other words, when the section radius is very sensitive to the performance and mass, if the design variable is optimized, the BCCZ lattice structure performance will be improved as well as the BCCZ lattice structure mass. That is, the reason for the BCCZ lattice structure performance improvement may be achieved by adding materials, which violates the original optimization intention of greatly improving the material utilization. In this paper, the concept of specific sensitivity is introduced to find out the performance sensitivity of design variables under unit mass and the mass sensitivity of design variables under unit performance.

In this paper, the specific sensitivity is defined as the ratio of the sensitivity of the BCCZ lattice structure performance to the pillar section radius and the sensitivity of the BCCZ lattice structure mass to the pillar section radius, namely:

$$\eta_i = \frac{\varepsilon_i}{\alpha_i} \quad (7)$$

where η_i is the specific sensitivity, ε_i is the performance sensitivity and α_i is the mass sensitivity.

Because it is difficult to obtain the sensitivity value directly through the theoretical formula, at the same time, there is a complex stress concentration phenomenon at the node of the BCCZ lattice structure, and the coupling between design variables is also complex, there are many problems and difficulties in applying the analytical method directly [41,42]. Therefore, this paper used finite element analysis tools to extract the values of performance sensitivity and mass sensitivity. The following example is to illustrate the method.

According to Formula (6), if the variable is x_i , the performance function is p_i ; when the variable is increased by one unit, the performance function corresponding to x_{i+1} is p_{i+1} .

$$\begin{cases} dP = p_{i+1} - p_i \\ dx_i = x_{i+1} - x_i = 1 \end{cases} \quad (8)$$

That is, when the mass unit changes,

$$\varepsilon_i = \frac{\partial p}{\partial x_i} = dP \quad (9)$$

The values of p_{i+1} and p_i are extracted by finite element analysis tools, and the performance sensitivity value of any design variable x_i can be obtained by Formulas (8) and (9).

The mass sensitivity can also be obtained by the above method, and the specific sensitivity can be obtained by Formula (7). At the same time, in order to make the specific sensitivity value more accurate, this paper obtains the final specific sensitivity value by setting multiple groups of data and curve fitting multiple groups of results. According to the specific sensitivity value obtained, the optimal design scheme can be further formulated on the basis of determining the design variables. Its purpose is:

- (1) Increasing the design variable with the maximum specific sensitivity can achieve the maximum performance improvement with the minimum mass increase.
- (2) Reducing the design variable with the minimum specific sensitivity can achieve the minimum performance degradation with the maximum mass reduction.

3.2. Imitative Full Stress Optimization Method

Through the analysis of Section 3.1, the design variables and their optimization directions can be determined, and the optimization design scheme can be preliminarily obtained. For the design variables to be optimized, this paper refers to the idea of imitative full stress design and proposes an optimization method for the cross section dimensions of each

pillar of the BCCZ lattice structure. The basic idea of imitative full stress is to make the most unfavorable stress in structural members approach or reach the allowable stress of materials, so as to make full use of materials. The mathematical model of this method is established as follows.

1. Optimization design variables: the BCCZ lattice structure section radius r_i of inclined pillar and section radius r'_i of outer pillar.

$$R = (r_1, \dots, r_m, r'_1, \dots, r'_n) \quad (10)$$

2. Objective function: the overall mass of the BCCZ lattice structure. The objective of optimization is to minimize the objective function.

$$\min W \approx \frac{\sqrt{3}}{2} \sum_{i=1}^m \pi r_i^2 S + \sum_{i=1}^n \pi r'_i{}^2 S \quad (11)$$

3. Constraint 1: the strength of each pillar approximates the allowable stress value.

$$C(x) = \sigma_{imax} - [\sigma_i] \cong 0 \quad (12)$$

In the formula, \cong is a symbol to describe the imitative full stress, which means that the value on the left of the symbol is infinitely close to but not more than the value on the right of the symbol, σ_{imax} is the maximum von Mises stress of pillar i under a certain condition, and $[\sigma_i]$ is the allowable stress of pillar materials of the BCCZ lattice structure.

4. Constraint 2: The value range of each pillar radius of the BCCZ lattice structure shall be between the minimum manufacturing size and the maximum space size of AM.

$$\begin{cases} r_{imin} \leq r_i \leq r_{imax} \\ r'_{imin} \leq r'_i \leq r'_{imax} \end{cases} \quad (13)$$

where r_{imin} and r'_{imin} are the minimum manufacturing dimensions of AM, set as 0.5 mm according to [24,25,43], and r_{imax} and r'_{imax} are the maximum space dimensions of AM. Considering the application scope of the pillar, 30% of the pillar length is selected as the upper limit of the section radius.

Therefore, the steps of the imitative full stress optimization method in this paper are as follows.

1. In the initial stage, set a reasonable set of section radius of each pillar.

$$R^0 = \{r_1^0, \dots, r_m^0, r'_1{}^0, \dots, r'_n{}^0\} \quad (14)$$

where R^0 represents the set of initial section radius of each pillar, and r_i^0 ($r'_i{}^0$) represents the initial value of pillar i .

2. Structural analysis. Similar to the difficulties encountered in applying the analytical method to the specific sensitivity analysis, this paper chooses to use the finite element analysis tool to obtain the maximum von Mises stress value and the minimum von Mises stress value of each pillar of the BCCZ lattice structure, namely σ_{imax} and σ_{imin} , and sort them in descending and ascending order, respectively, and set

$$\begin{cases} \sigma_{max} = \max\{\sigma_{imax}\} (i = 1, 2, \dots, m + n) \\ \sigma_{min} = \min\{\sigma_{imin}\} (i = 1, 2, \dots, m + n) \end{cases} \quad (15)$$

where σ_{max} and σ_{min} are the maximum von Mises stress and minimum von Mises stress of the BCCZ lattice structure as a whole, respectively.

3. Strength verification. Compare the σ_{max} obtained in step 2 with the allowable stress $[\sigma_i]$, and enter the corresponding iteration cycles 4 and 5 according to the comparison results.
4. When $\sigma_{max} > [\sigma_i]$, it indicates that the overall strength of the BCCZ lattice structure under the current section radius of each pillar is too large, and the section radius of the pillar where the maximum von Mises stress is located must be increased, and then go to step 2 again to update the structural analysis results. When the condition $\sigma_{max} \leq [\sigma_i]$ is met, jump out of the cycle and output the value of the current section radius of each pillar. If the end of cycle condition cannot be satisfied all the time, the optimization is terminated because there is no feasible solution to the problem.
5. When $\sigma_{max} \leq [\sigma_i]$, it indicates that the materials of some pillars may not be fully utilized under the current section radius of each pillar, so it is necessary to find out the corresponding pillar and reduce the section radius of the corresponding pillar, and turn to step 2 again. According to the new structure analysis results, it can be divided into the following two cases:
 - (1) $\sigma_{max} \leq [\sigma_i]$: It shows that the material is still not fully utilized under the current section radius of each pillar, so the section radius of the pillar where the current minimum von Mises stress is located must be reduced, and go to step 2. If $\sigma_{max} \leq [\sigma_i]$ is still satisfied until the minimum value of the optimization variable is obtained, the minimum value is output.
 - (2) $\sigma_{max} > [\sigma_i]$: It shows that the pillar with the reduced section radius in the previous step has reached the material utilization limit. It is necessary to sort out the results of the structural analysis in the previous step according to the minimum von Mises stress value, find the pillar with the next von Mises stress and reduce its section radius, and then turn to step 2. If the section radius of all optimized pillars is reduced once by continuous traversal, the cycle will be skipped and the section radius of each pillar meeting $\sigma_{max} \leq [\sigma_i]$ will be output.
6. The values of each pillar obtained in Cycle 4 and Cycle 5 constitute the final optimization results.

$$R^m = \{r_1^u, \dots, r_m^u, r_5^v, \dots, r_n^v\} \tag{16}$$

where u and v are the number of iterations in the two cycles, respectively.

Figure 6 shows the step flow chart of the imitative full stress optimization method.

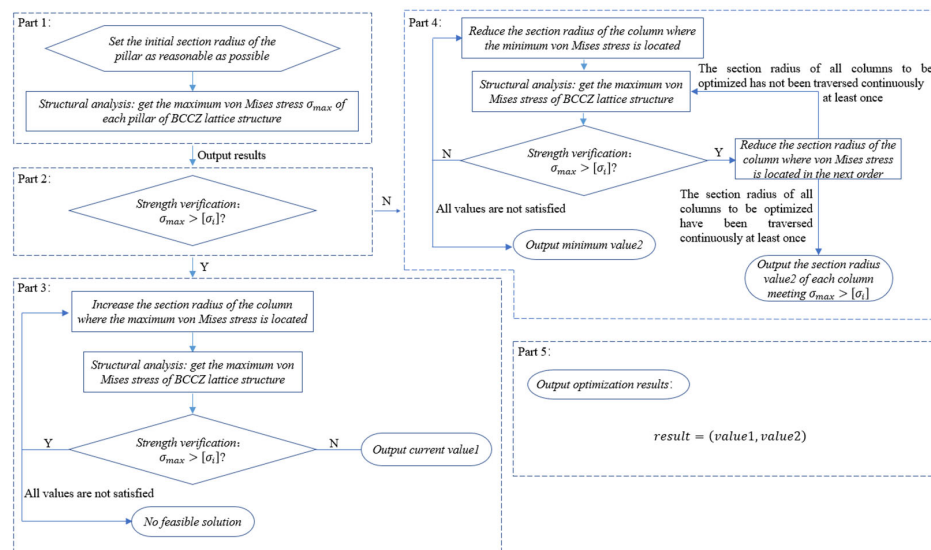


Figure 6. Flow chart of imitative full stress optimization method.

4. Example

4.1. Models for the Test

In this paper, numerical examples are given to verify the effectiveness of the proposed optimization method for the BCCZ lattice structure parameters. The optimization goal is to improve the compressive strength of the test model. As unit cell is very representative in the study of lattice structure, the BCCZ unit cell was selected as a test case to illustrate. The BCCZ unit cell size was set as 5 mm, the initial section radius of each pillar was 0.5 mm, and the allowable stress $[\sigma_i]$ was set as 120 MPa. The numbering sequence of the BCCZ unit cell is shown in Figure 3. The BCCZ unit cell numerical model was designed based on this, and the model diagram is shown in Figure 7.

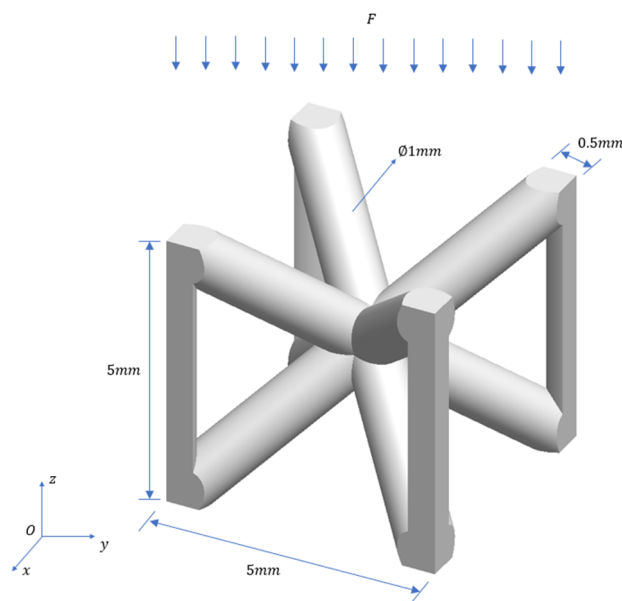


Figure 7. Test case—BCCZ unit cell initial model.

4.2. Optimization Results

According to the analysis conclusion in Section 2.2, the BCCZ unit cell test case was analyzed for specific sensitivity, and each pillar was taken as an independent variable to evaluate the impact of the section radius of each pillar on the overall performance. The results of specific sensitivity from pillar P1 to pillar P12 are shown in Table 1.

Table 1. Specific sensitivity η_i result of pillars P1 to P12.

Pillar	η_i
P1	−0.37
P2	−0.12
P3	−0.47
P4	−0.32
P5	−0.39
P6	−0.13
P7	−0.63
P8	−0.39
P9	−2.06
P10	−3.88
P11	−5.18
P12	−4.97

According to the specific sensitivity analysis results shown in Table 1, the following optimization design scheme can be obtained according to the specific sensitivity analysis results processing method in Section 3.1.

- (1) The section radius of P1–P8 is reduced, so that the mass of BCCZ unit cell is reduced without great influence on the strength of the BCCZ unit cell.
- (2) Increase the section radius of P9–P12 so as to improve the strength of BCCZ unit cell under the condition that the mass of BCCZ unit cell is basically unchanged.

According to the above design scheme, the optimization of the BCCZ unit cell can be divided into two directions. First, the initial BCCZ unit cell was analyzed by the finite element method. At this time, the maximum equivalent stress was greater than the allowable stress. The BCCZ unit cell strength needs to be improved according to the optimal design scheme (2). After the imitative full stress optimization iteration at this stage, the section radius of the pillars P9–P12 was increased, making the maximum equivalent stress less than the allowable stress, so that the test case met the strength requirements. Secondly, after the strength requirements were met, the pursuit of minimizing the overall mass was started. At this time, the mass of BCCZ unit cell should be reduced according to the optimal design scheme (1) under the framework where the maximum equivalent stress is less than the allowable stress. After the imitative full stress optimization iteration at this stage, the minimum section radius of the P1–P8 pillars under the strength requirements was calculated. Finally, the optimization results of the two stages were combined to output the optimization results of the imitative full stress of pillars P1–P12. The final optimization results are shown in Table 2 and Figure 8.

Table 2. Results of BCCZ unit cell optimized by imitative full stress.

Pillar	Section Radius (mm)
P1	1.1
P2	1.3
P3	1.1
P4	1.3
P5	1
P6	0.9
P7	1
P8	0.9
P9	1
P10	0.9
P11	1
P12	0.9

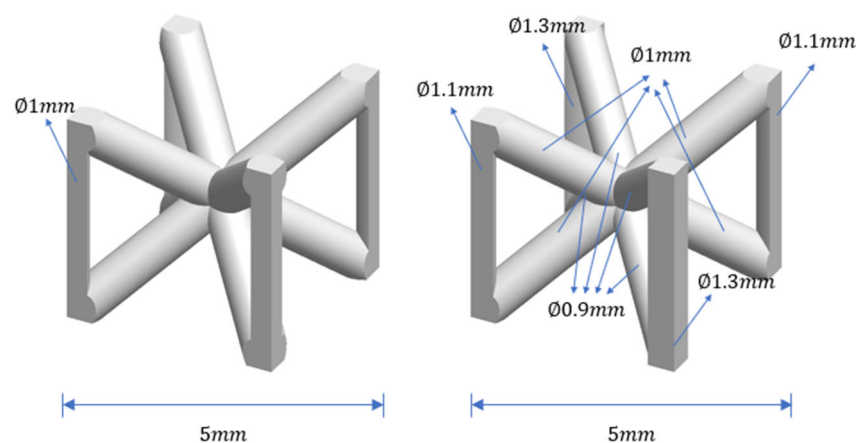


Figure 8. BCCZ unit cell comparison before and after imitative full stress optimization.

5. Numerical Simulation and Experimental Verification

In order to verify the effectiveness of the proposed optimization method, the optimized BCCZ unit cell obtained in Section 4.2 was simulated and verified by experiments. In terms of the manufacturing of experimental samples, Yu et al. [44], Tang et al. [45] and Dong et al. [46] used, respectively, the electron beam powder bed fusion (EBPBF), binder jetting (BJ) and fused deposition modeling (FDM) techniques to manufacture corresponding experimental samples for their own research experiments. In order to ensure that the samples have high accuracy, this paper selected LPBF technology to manufacture the corresponding experimental samples. In recent years, AlSi₁₀Mg material has been used more and more for the fabrication of AM'ed parts, which has good molding effect and cheaper cost, and low-density and high strength. At the same time, it is suitable for manufacturing lattice structures [24,47]. The experimental sample in this paper was formed by LPBF with a light weight structure, considering the economic rationality. Therefore, light material AlSi₁₀Mg alloy powder with good welding formability, thermal conductivity and corrosion resistance was selected [7]. The chemical composition and physicomechanical properties of the AlSi₁₀Mg alloy powder used for simulation and experiment are shown in Tables 3 and 4.

Table 3. Chemical composition of AlSi₁₀Mg.

Material	Main Elements						Impurity				
	Al	Si	Mg	Fe	Cu	Mn	Ni	Zn	Pb	Sn	Ti
AlSi ₁₀ Mg	bal	11.7	0.39	0.15	0.05	0.45	0.05	0.10	0.05	0.05	0.15

Table 4. Physicomechanical properties of AlSi₁₀Mg.

Material	Density [kg/m ³]	Young's Modulus [MPa]	Yield Strength [MPa]
AlSi ₁₀ Mg	2670	75,000	350

5.1. Numerical Simulation

In order to compare with the experiment and simulate the quasi-static compression process in the actual experiment, this paper designed the BCCZ unit cell simulation model before and after optimization, as shown in Figure 9. The pressing plate was set at both ends of the BCCZ unit cell to simulate the pressure head in the experiment, and the ANSYS Workbench was used for simulation analysis.

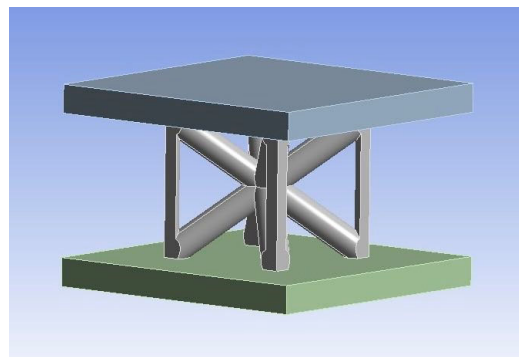


Figure 9. Simulation model of BCCZ unit cell.

According to the experimental conditions of quasi-static compression, the BCCZ unit cell and the compression platform were in static friction contact during compression, and the friction coefficient between metals was 0.15. The upper platen applied a one-way vertical displacement load of 1.5 mm, the lower platen was set as a fixed constraint, and

large deformation was opened during simulation. After the use of the ANSYS intelligent grid division, through comparison, it was found that further increasing the number of grids had little impact on the simulation results. This showed that the grid was independent at this time, so this paper used the intelligent grid generation function of ANSYS for simulation analysis. The results of the simulation analysis are shown in Table 5.

Table 5. Simulation analysis results of BCCZ unit cell before and after optimization.

BCCZ	Strength Limit (MPa)		
	Initial	After optimization	Optimize efficiency
	668.72	794.22	18.77%

5.2. Sample Preparation

The LiM-X260A metal 3D printer produced by Tianjin LiM Laser Technology Co., Ltd. (Tianjin, China) was selected as the experimental equipment for manufacturing experimental samples, and the equipment is shown in Figure 10. The equipment has the advantages of high precision, high forming efficiency, high automation, high reliability, high efficiency and stability. Table 6 shows the process manufacturing parameters of manufacturing samples. During manufacturing, the outer pillars of the samples were placed vertically with the printing plane, as shown in Figure 11.

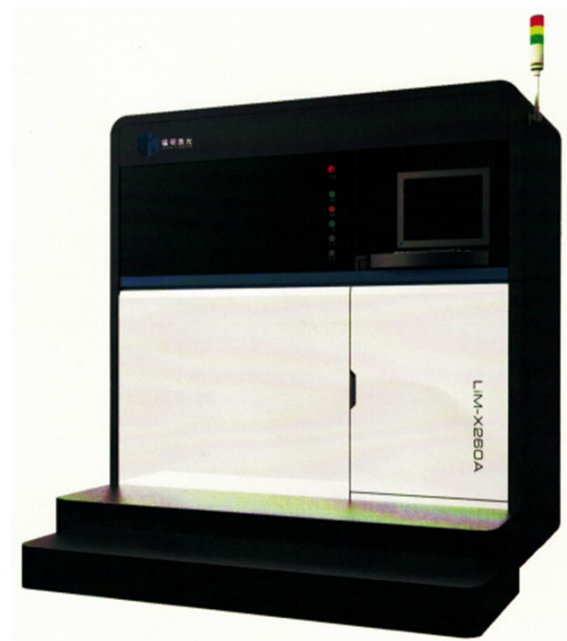


Figure 10. LiM-X260A metal 3D printer produced by Tianjin LiM Laser Technology Co., Ltd.

Table 6. Process parameters for sample manufacturing.

Process Parameters	Numerical Value
Laser power	370 W
Delamination thickness	30 μm
Scanning speed	1300 mm/s
Laser wavelength	1060~1080 nm
Spot diameter	85 μm
Oxygen content	≤ 1000 ppm

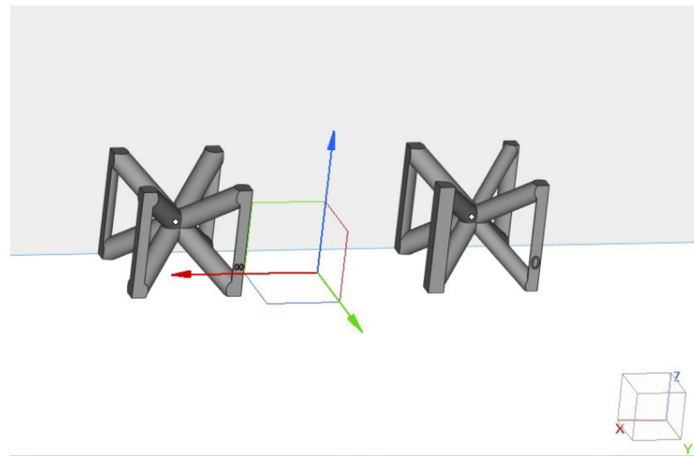


Figure 11. Schematic diagram of sample placement during AM. Left: before optimization, Right: after optimization.

We printed three experimental samples for each digital model, and the BCCZ unit cell structure physical diagram manufactured by the LPBF process is shown in Figure 12. The overall printing of the sample was complete, and there was no incomplete phenomenon such as bar fracture. According to the measurement, all dimensions were consistent with the theoretical dimensions.



Figure 12. Printed sample.

5.3. Experimental Process and Results

For the experimental samples manufactured by LPBF technology, the WDW-20 electronic universal testing machine was selected for a quasi-static compression test to quantify the compressive strength of the BCCZ unit cells [48]. During the compression test, we set the loading speed of the indenter to 1 mm/min to simulate the quasi-static conditions. In the software, we set the force sensor to detect that the force reached 0.001 KN and recorded the deformation data. During the test, we observed the load displacement curve and recorded the test process with a camera. When the sample was about to be compacted, we stopped the machine and saved the experimental data. Figure 13 shows the experimental process of the compression experiment.

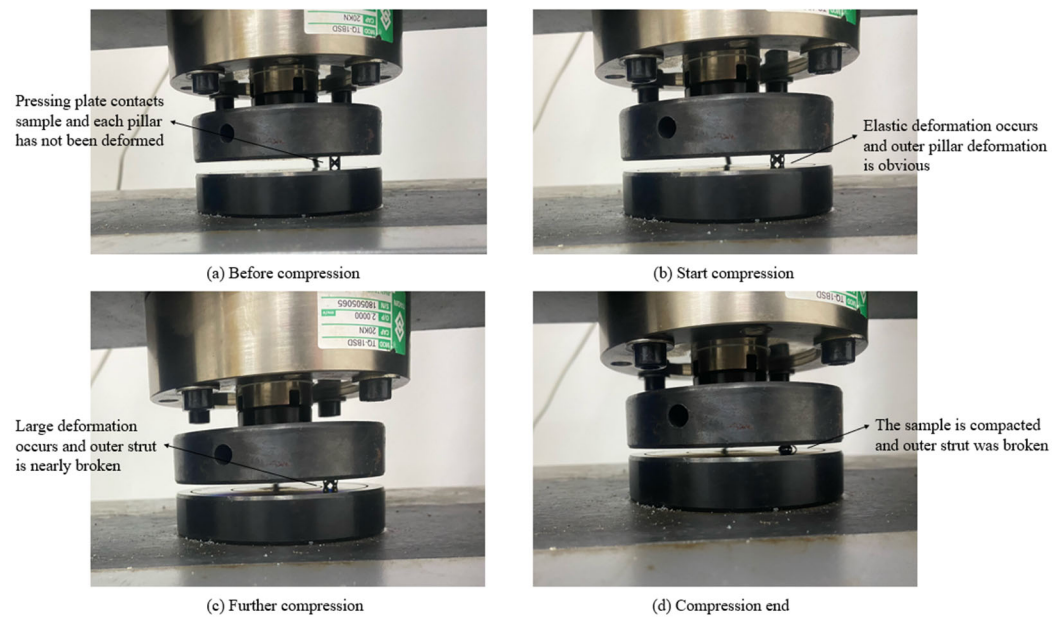


Figure 13. Experimental process of quasi-static compression experiment.

In the compression experiment, the BCCZ unit cell was deformed due to the falling of the pressing plate, and these results were obtained through the sensor. At the same time, the load at each moment could be captured through the force sensor, so that multiple groups of corresponding experimental data could be obtained. All the compression experiments were completed, and the load displacement curve was drawn after sorting out several groups of experimental data. In this paper, the contact area between the compression platform and the sample was read through the theoretical model. After processing, the stress–strain curve of the sample before and after optimization was obtained. For the same type of BCCZ unit cell model, three repeated tests were carried out, and it was found that the curve change trend of the three experiments was basically consistent. Figure 14 shows the stress–strain response of the BCCZ unit cell under compression before and after optimization.

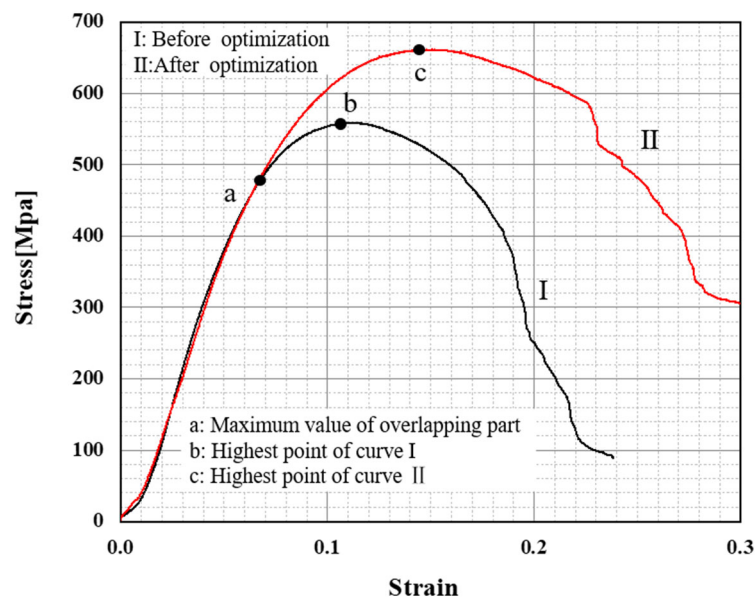


Figure 14. Stress–strain curves of BCCZ unit cell before and after optimization obtained through quasi-static compression experiments. Black: before optimization, it corresponds to Figure 8 (left); Red: after optimization, it corresponds to Figure 8 (right).

The following conclusions can be drawn by observing the stress–strain curve shown in Figure 14:

- The BCCZ unit cell compression mainly goes through four stages: linear elastic stage, yield stage, strengthening stage and failure stage. The origin in Figure 14 corresponds to the state shown in Figure 13a;
- The material is linear elastic. When the elastic modulus reaches the elastic limit, the BCCZ cell begins to yield plastic. At the Oa curve, the stress–strain curves of BCCZ cells before and after optimization are basically consistent. This stage corresponds to Figure 13b;
- The maximum compressive strength limit (point c) of the BCCZ unit cell after optimization is significantly higher than that of the BCCZ unit cell before optimization (point b), which indicates that the strength of the BCCZ unit cell obtained through the optimization method in this paper has been improved, and the optimization method in this paper has an obvious effect on strength optimization. The specific data are shown in Table 7;
- The BCCZ unit cell will have curve fluctuation in the later failure stage, which may be caused by the alternate fracture of the strengthened Z pillar. This stage corresponds to Figure 13c,d.

Table 7. Comparison of strength and mass of BCCZ cells before and after optimization after three quasi-static compression tests.

	Strength Limit (MPa)			Mass (10–5 kg)		
	Initial	After optimization	Optimize efficiency	Initial	After optimization	Optimize efficiency
BCCZ	558.40	661.31	18.43%	6.64	6.47	0.03%

6. Conclusions

In order to solve the problem of uniform pillar thickness and uneven stress distribution in the BCCZ lattice structure, so as to better play the performance advantages of the BCCZ lattice structure in light weight and high strength, and improve the utilization rate of materials. This paper proposes an optimization method of BCCZ lattice structure based on parametric modeling parameters. The main work of this paper is as follows.

- (1) The structural parameters of the BCCZ lattice structure are analyzed. From the perspective of a unit cell, the construction elements of BCCZ lattice structure are explored, and it is concluded that the necessary elements for BCCZ lattice structure modeling are cell side length S , section radius r_i ($i = 1, 2, \dots, 8$) of inclined pillar, section radius r'_i ($i = 9, 10, 11, 12$) of outer pillar, X , Y , and the number of cells in Z direction x , y and z . Through the above construction elements, the BCCZ lattice structure model can be built.
- (2) Taking the construction parameters of the BCCZ lattice structure as independent variables, the finite element analysis method is used to reduce the influence of stress concentration at the nodes of the BCCZ lattice structure and simplify the calculation of the interaction between variables. Assuming that the cell side length S is unchanged, the section radius of each pillar of BCCZ lattice structure is optimized. The specific sensitivity analysis is used to simplify the number of design variables and give the optimization directions of different design variables. The subsequent optimization design scheme is given according to the specific sensitivity analysis results. Based on the optimization design scheme and the idea of imitative full stress, the BCCZ lattice structure is iterated for strength optimization to improve the material utilization rate of the BCCZ lattice structure and obtain the optimal section radius of each pillar in the structure.
- (3) A test case is designed to verify the optimization method. BCCZ unit cell is selected for the test case, with the goal of improving its compressive strength. The simulation

and quasi-static compression experiments are used to compare the BCCZ unit cell before and after optimization. The comparison results show that the strength limit of the BCCZ unit cell after optimization is increased by 18.77% and 18.43%, respectively, indicating that the optimization results have strong consistency.

The advantage of the optimization method in this paper is that the stress can be selected according to the setting, and the results of the section radius of each pillar of BCCZ lattice structure with the minimum mass meeting the strength requirements can be output. In the test case in this paper, the objective of simulation is compressive strength. Under other load conditions, the optimization method in this paper also has reference value. Besides the BCCZ lattice structure, this optimization method can also be used for reference for other node structure lattice structures. In addition, the experimental results of this optimization method also prove the advantages of non-uniform design, and non-uniform lattice structures can have higher strength than uniform lattice structures. These two kinds of situations will be considered in our next work.

Author Contributions: Conceptualization, H.L. and W.Y.; methodology, H.L.; validation, H.L. and Z.Q.; formal analysis, Q.M. and H.L.; investigation, H.L. and Z.Q.; resources, W.Y.; writing—original draft preparation, H.L. and Q.M.; writing—review and editing, W.Y. and L.Y.; supervision, W.Y.; funding acquisition, W.Y. All authors have read and agreed to the published version of the manuscript.

Funding: The authors are thankful for the support from the National Natural Science Foundation of China, under the Grant No. 52175313, and Key Science and Technology Project of Hebei Province, China, under the Grant No. 21284901Z.

Data Availability Statement: Not applicable.

Acknowledgments: These experiments were completed in the Advanced Materials Testing and Analysis Center of HEBUT. At the same time, thanks to the scientific research platform provided by the National Engineering Research Center for Technical Innovation Method and Tool. The authors thank them for their help.

Conflicts of Interest: The authors declare no conflict of interest.

References

1. Guo, N.; Leu Ming, C. Additive manufacturing: Technology, applications and research needs. *Front. Mech. Eng.* **2013**, *8*, 215–243. [[CrossRef](#)]
2. Gu, D.D.; Shi, X.Y.; Poprawe, R.; Bourell, D.L.; Setchi, R.; Zhu, J.H. Material-structure-performance integrated laser-metal additive manufacturing. *Science* **2021**, *372*, eabg1487. [[CrossRef](#)] [[PubMed](#)]
3. Safavi, M.S.; Bordbar-Khiabani, A.; Khalil-Allafi, J.; Mozafari, M.; Visai, L. Additive Manufacturing: An Opportunity for the Fabrication of Near-Net-Shape NiTi Implants. *J. Manuf. Mater. Process.* **2022**, *6*, 65. [[CrossRef](#)]
4. Sing, S.L. Perspectives on Additive Manufacturing Enabled Beta-Titanium Alloys for Biomedical Applications. *Int. J. Bioprint.* **2022**, *8*, 478. [[CrossRef](#)]
5. Zhang, H.; Gu, D.; Dai, D. Laser printing path and its influence on molten pool configuration, microstructure and mechanical properties of laser powder bed fusion processed rare earth element modified Al-Mg alloy. *Virtual Phys. Prototyp.* **2022**, *17*, 308–328. [[CrossRef](#)]
6. Maonachie, T.; Leary, M.; Tran, P.; Harris, J.; Liu, Q.; Lu, G.X.; Ruan, D.; Faruque, O.; Brandt, M. The effect of topology on the quasi-static and dynamic behaviour of SLM AlSi10Mg lattice structures. *Int. J. Adv. Manuf. Technol.* **2022**, *118*, 4085–4104. [[CrossRef](#)]
7. Aboulkhair, N.T.; Simonelli, M.; Parry, L.; Ashcroft, I.; Tuck, C.; Hague, R. 3D printing of Aluminium alloys: Additive Manufacturing of Aluminium alloys using selective laser melting. *Prog. Mater. Sci.* **2019**, *106*, 45. [[CrossRef](#)]
8. Kumar, A.; Collini, L.; Daurel, A.; Jeng, J.Y. Design and additive manufacturing of closed cells from supportless lattice structure. *Addit. Manuf.* **2020**, *33*, 10. [[CrossRef](#)]
9. Vaissier, B.; Pernot, J.P.; Chougrani, L.; Veron, P. Parametric design of graded truss lattice structures for enhanced thermal dissipation. *Comput. Aided Des.* **2019**, *115*, 1–12. [[CrossRef](#)]
10. Al-Saedi, D.S.J.; Masood, S.H.; Faizan-Ur-Rab, M.; Alomarah, A.; Ponnusamy, P. Mechanical properties and energy absorption capability of functionally graded F2BCC lattice fabricated by SLM. *Mater. Des.* **2018**, *144*, 32–44. [[CrossRef](#)]
11. Catchpole-Smith, S.; Selo, R.R.J.; Davis, A.W.; Ashcroft, I.A.; Tuck, C.J.; Clare, A. Thermal conductivity of TPMS lattice structures manufactured via laser powder bed fusion. *Addit. Manuf.* **2019**, *30*, 9. [[CrossRef](#)]

12. Chen, Y.; Zhao, B.H.; Liu, X.N.; Hu, G.K. Highly anisotropic hexagonal lattice material for low frequency water sound insulation. *Extreme Mech. Lett.* **2020**, *40*, 7. [[CrossRef](#)]
13. Zhang, L.C.; Chen, L.Y. A Review on Biomedical Titanium Alloys: Recent Progress and Prospect. *Adv. Eng. Mater.* **2019**, *21*, 29. [[CrossRef](#)]
14. Tamburrino, F.; Graziosi, S.; Bordegoni, M. The Design Process of Additively Manufactured Mesoscale Lattice Structures: A Review. *J. Comput. Inf. Sci. Eng.* **2018**, *18*, 040801. [[CrossRef](#)]
15. Cutolo, A.; Engelen, B.; Desmet, W.; Van Hooreweder, B. Mechanical properties of diamond lattice Ti-6Al-4V structures produced by laser powder bed fusion: On the effect of the load direction. *J. Mech. Behav. Biomed. Mater.* **2020**, *104*, 11. [[CrossRef](#)] [[PubMed](#)]
16. Vrana, R.; Jaros, J.; Koutny, D.; Nosek, J.; Zikmund, T.; Kaiser, J.; Palousek, D. Contour laser strategy and its benefits for lattice structure manufacturing by selective laser melting technology. *J. Manuf. Process.* **2022**, *74*, 640–657. [[CrossRef](#)]
17. Vuksanovich, B.; Gygi, C.; Cortes, P.; Chavez, J.; MacDonald, E.; Ohara, R.; Du Plessis, A. Non-Destructive Inspection of Sacrificial 3D Sand-Printed Molds with Geometrically Complex Lattice Cavities. *Int. J. Met.* **2022**, *16*, 1091–1100. [[CrossRef](#)]
18. Jia, D.J.; Li, F.C.; Zhang, Y. 3D-printing process design of lattice compressor impeller based on residual stress and deformation. *Sci. Rep.* **2020**, *10*, 11. [[CrossRef](#)]
19. Yin, S.; Chen, H.Y.; Wu, Y.B.; Li, Y.B.; Xu, J. Introducing composite lattice core sandwich structure as an alternative proposal for engine hood. *Compos. Struct.* **2018**, *201*, 131–140. [[CrossRef](#)]
20. du Plessis, A.; Yadroitsava, I.; Yadroitsev, I.; le Rouxa, S.G.; Blaine, D.C. Numerical comparison of lattice unit cell designs for medical implants by additive manufacturing. *Virtual Phys. Prototyp.* **2018**, *13*, 266–281. [[CrossRef](#)]
21. Abdulhameed, O.; Al-Ahmari, A.; Ameen, W.; Mian, S.H. Additive manufacturing: Challenges, trends, and applications. *Adv. Mech. Eng.* **2019**, *11*, 27. [[CrossRef](#)]
22. Wang, J.; Li, Y.; Hu, G.; Yang, M.S. Lightweight Research in Engineering: A Review. *Appl. Sci.* **2019**, *9*, 24. [[CrossRef](#)]
23. Lei, H.S.; Li, C.L.; Meng, J.X.; Zhou, H.; Liu, Y.B.; Zhang, X.Y.; Wang, P.D.; Fang, D.N. Evaluation of compressive properties of SLM-fabricated multi-layer lattice structures by experimental test and mu-CT-based finite element analysis. *Mater. Des.* **2019**, *169*, 15. [[CrossRef](#)]
24. Leary, M.; Mazur, M.; Elambasseril, J.; McMillan, M.; Chirent, T.; Sun, Y.; Qian, M.; Easton, M.; Brandt, M. Selective laser melting (SLM) of AlSi12Mg lattice structures. *Mater. Des.* **2016**, *98*, 344–357. [[CrossRef](#)]
25. Leary, M.; Mazur, M.; Williams, H.; Yang, E.; Alghamdi, A.; Lozanovski, B.; Zhang, X.Z.; Shidid, D.; Farahbod-Sternahl, L.; Witt, G.; et al. Inconel 625 lattice structures manufactured by selective laser melting (SLM): Mechanical properties, deformation and failure modes. *Mater. Des.* **2018**, *157*, 179–199. [[CrossRef](#)]
26. Maskery, I.; Hussey, A.; Panesar, A.; Aremu, A.; Tuck, C.; Ashcroft, I.; Hague, R. An investigation into reinforced and functionally graded lattice structures. *J. Cell. Plast.* **2017**, *53*, 151–165. [[CrossRef](#)]
27. Wang, S.; Wang, J.; Xu, Y.J.; Zhang, W.H.; Zhu, J.H. Compressive behavior and energy absorption of polymeric lattice structures made by additive manufacturing. *Front. Mech. Eng.* **2020**, *15*, 319–327. [[CrossRef](#)]
28. Umer, R.; Barsoum, Z.; Jishi, H.Z.; Ushijima, K.; Cantwell, W.J. Analysis of the compression behaviour of different composite lattice designs. *J. Compos. Mater.* **2018**, *52*, 715–729. [[CrossRef](#)]
29. Chua, C.; Sing, S.L.; Chua, C.K. Characterisation of in-situ alloyed titanium-tantalum lattice structures by laser powder bed fusion using finite element analysis. *Virtual Phys. Prototyp.* **2022**, *18*, e2138463. [[CrossRef](#)]
30. Chen, W.; Zheng, X.; Liu, S. Finite-Element-Mesh Based Method for Modeling and Optimization of Lattice Structures for Additive Manufacturing. *Materials* **2018**, *11*, 2073. [[CrossRef](#)]
31. Jin, X.; Li, G.X.; Zhang, M. Optimal design of three-dimensional non-uniform nylon lattice structures for selective laser sintering manufacturing. *Adv. Mech. Eng.* **2018**, *10*, 1687814018790833. [[CrossRef](#)]
32. Chen, L.-Y.; Liang, S.-X.; Liu, Y.; Zhang, L.-C. Additive manufacturing of metallic lattice structures: Unconstrained design, accurate fabrication, fascinated performances, and challenges. *Mater. Sci. Eng. R Rep.* **2021**, *146*, 100648. [[CrossRef](#)]
33. Zargarian, A.; Esfahanian, M.; Kadkhodapour, J.; Ziaei-Rad, S.; Zamani, D. On the fatigue behavior of additive manufactured lattice structures. *Theor. Appl. Fract. Mech.* **2019**, *100*, 225–232. [[CrossRef](#)]
34. Li, P.Y.; Ma, Y.E.; Sun, W.B.; Qian, X.D.; Zhang, W.H.; Wang, Z.H. Fracture and failure behavior of additive manufactured Ti6Al4V lattice structures under compressive load. *Eng. Fract. Mech.* **2021**, *244*, 12. [[CrossRef](#)]
35. Zhao, M.; Zhang, D.Z.; Li, Z.H.; Zhang, T.; Zhou, H.L.; Ren, Z.H. Design, mechanical properties, and optimization of BCC lattice structures with taper struts. *Compos. Struct.* **2022**, *295*, 15. [[CrossRef](#)]
36. Zhang, L.; Song, B.; Yang, L.; Shi, Y.S. Tailored mechanical response and mass transport characteristic of selective laser melted porous metallic biomaterials for bone scaffolds. *Acta Biomater.* **2020**, *112*, 298–315. [[CrossRef](#)] [[PubMed](#)]
37. Liu, Y.; Zhuo, S.R.; Xiao, Y.N.; Zheng, G.L.; Dong, G.Y.; Zhao, Y.F. Rapid Modeling and Design Optimization of Multi-Topology Lattice Structure Based on Unit-Cell Library. *J. Mech. Des.* **2020**, *142*, 15. [[CrossRef](#)]
38. Niu, X.P.; Wang, R.Z.; Liao, D.; Zhu, S.P.; Zhang, X.C.; Keshtegar, B. Probabilistic modeling of uncertainties in fatigue reliability analysis of turbine bladed disks. *Int. J. Fatigue* **2021**, *142*, 11. [[CrossRef](#)]
39. Tang, Y.; Dong, G.; Zhou, Q.; Zhao, Y.F. Lattice Structure Design and Optimization With Additive Manufacturing Constraints. *IEEE Trans. Autom. Sci. Eng.* **2018**, *15*, 1546–1562. [[CrossRef](#)]
40. Xu, Y.L.; Li, T.T.; Cao, X.Y.; Tan, Y.Q.; Luo, P.H. Compressive Properties of 316L Stainless Steel Topology-Optimized Lattice Structures Fabricated by Selective Laser Melting. *Adv. Eng. Mater.* **2021**, *23*, 15. [[CrossRef](#)]

41. Li, D.; Qin, R.; Xu, J.; Zhou, J.; Chen, B. Improving Mechanical Properties and Energy Absorption of Additive Manufacturing Lattice Structure by Struts' Node Strengthening. *Acta Mech. Solida Sin.* **2022**, 1–17. [[CrossRef](#)]
42. Mokryakov, V.V. Strength analysis of an elastic plane containing a square lattice of circular holes under mechanical loading. *Mech. Solids* **2014**, *49*, 568–577. [[CrossRef](#)]
43. Tanlak, N.; De Lange, D.F.; Van Paepegem, W. Numerical prediction of the printable density range of lattice structures for additive manufacturing. *Mater. Des.* **2017**, *133*, 549–558. [[CrossRef](#)]
44. Yu, G.J.; Li, X.; Dai, L.S.; Xiao, L.J.; Song, W.D. Compressive properties of imperfect Ti-6Al-4V lattice structure fabricated by electron beam powder bed fusion under static and dynamic loadings. *Addit. Manuf.* **2022**, *49*, 18. [[CrossRef](#)]
45. Tang, Y.; Zhou, Y.; Hoff, T.; Garon, M.; Zhao, Y.F. Elastic modulus of 316 stainless steel lattice structure fabricated via binder jetting process. *Mater. Sci. Technol.* **2016**, *32*, 648–656. [[CrossRef](#)]
46. Dong, G.Y.; Wijaya, G.; Tang, Y.L.; Zhao, Y.F. Optimizing process parameters of fused deposition modeling by Taguchi method for the fabrication of lattice structures. *Addit. Manuf.* **2018**, *19*, 62–72. [[CrossRef](#)]
47. Martin, J.H.; Yahata, B.D.; Hundley, J.M.; Mayer, J.A.; Schaedler, T.A.; Pollock, T.M. 3D printing of high-strength aluminium alloys. *Nature* **2017**, *549*, 365–369. [[CrossRef](#)]
48. Feng, Q.X.; Tang, Q.; Liu, Y.; Setchi, R.; Soe, S.; Ma, S.; Bai, L. Quasi-static analysis of mechanical properties of Ti6Al4V lattice structures manufactured using selective laser melting. *Int. J. Adv. Manuf. Technol.* **2018**, *94*, 2301–2313. [[CrossRef](#)]